

# Tertiary phosphine induced migratory carbonyl insertion in cyclopentadienyl complexes of iron(II)

Ntaoleng M. Makunya<sup>a,1</sup>, Reinout Meijboom<sup>b,\*</sup>, Alfred Muller<sup>b</sup>, Andreas Roodt<sup>b,\*</sup>

<sup>a</sup> Department of Chemistry, University of Johannesburg, P.O. Box 524, Auckland Park, 2006 Johannesburg, South Africa

<sup>b</sup> Department of Chemistry, University of the Free State, P.O. Box 339, 9300 Bloemfontein, South Africa

Received 12 May 2005; received in revised form 7 June 2005; accepted 20 June 2005

Available online 26 July 2005

## Abstract

Cyclopentadienyldicarbonylmethyliron,  $[\text{CpFe}(\text{CO})_2\text{Me}]$  (**1**), undergoes migratory carbonyl insertion under the influence of isoseric phosphine ligands  $\text{P}(4\text{-FC}_6\text{H}_4)_3$  and  $\text{P}(4\text{-MeC}_6\text{H}_4)_3$ . The products of the reaction,  $[\text{CpFe}(\text{CO})(\text{COMe})\text{P}(4\text{-FC}_6\text{H}_4)_3]$  (**2a**) and  $[\text{CpFe}(\text{CO})(\text{COMe})\text{P}(4\text{-MeC}_6\text{H}_4)_3]$  (**2b**), were characterised by X-ray crystallography. In both structures, the iron atom adopts a pseudo octahedral coordination geometry. Fe–P bond distances are the same at 2.1932(8) Å in **2a** and **2b**, respectively. Thus, contrary to what was expected, X-ray data could not be used to quantitatively differentiate between the two phosphine ligands in **2a** and **2b**. Therefore, additional spectroscopic techniques such as IR and NMR were employed. Similarly, the Fe–C bond lengths of the carbonyl (Fe–CO) and acetyl (Fe–COMe) are 1.748(3) and 1.955(3) in **2a**, and 1.744(3) and 1.951(3) Å in **2b**, respectively.

The migratory carbonyl insertion was studied by NMR, IR, and UV–vis spectroscopies to determine the mechanism and the rate law. Results from NMR spectroscopy show that the formation of the product is accompanied by oxidation of the corresponding phosphine ligand. An increase in the reactivity of migratory carbonyl insertion for  $\text{P}(4\text{-MeC}_6\text{H}_4)_3$  was observed when the solvent was changed from  $\text{CH}_2\text{Cl}_2$  to MeCN. The kinetic data showed that  $\text{P}(4\text{-MeC}_6\text{H}_4)_3$  reacts faster than  $\text{P}(4\text{-FC}_6\text{H}_4)_3$ .

© 2005 Elsevier B.V. All rights reserved.

**Keywords:** Iron; Migratory carbonyl insertion; X-ray crystallography; Kinetics

## 1. Introduction

Migratory carbonyl insertion serves as a key C–C bond formation pathway in catalytic carbonylations in the chemical industry, such as in the acetic acid synthesis from methanol with CO [1]. Transition metal alkyl and acyl compounds involved can be used as models for alkyl intermediates in the Fischer–Tropsch reactions. In general, Groups 8–10 metals are known to be active catalysts for the Fischer–Tropsch reaction, but to date only iron based catalysts are used industrially [2].

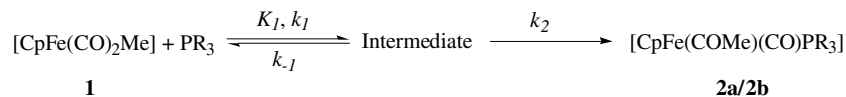
Factors known to govern the rate of migratory CO insertion reaction include the entering ligand [3], solvent [4,5] and alkyl group [6]. Ligand steric and electronic effects play a key role in determining organometallic reactivity trends and catalytic behavior. Phosphine based ligands have found widespread application both in organometallic chemistry and in industrial application of homogeneous catalysis, because their steric demands as well as their  $\sigma$ -donor and  $\pi$ -acceptor properties are subject to deliberate control [7]. For example, in the hydroformylation process, phosphine modified systems offer great benefits over unmodified systems, including increased catalyst stability [8], improved reaction rates and selectivity, and enhanced partitioning in two-phase systems [9].

Two main aspects are involved in the coordination of tertiary phosphine ligands to transition metal atoms.

\* Corresponding authors. Tel.: +27 51 401 2547; fax: +27 51 430 7805.

E-mail addresses: [meijboomr.sci@mail.uovs.ac.za](mailto:meijboomr.sci@mail.uovs.ac.za) (R. Meijboom), [roodta.sci@mail.uovs.ac.za](mailto:roodta.sci@mail.uovs.ac.za) (A. Roodt).

<sup>1</sup> Current address: Department of Chemistry, University of the Free State, P.O. Box 339, 9300 Bloemfontein, South Africa.



Scheme 1. General Scheme for the two-step reaction with a fast pre-equilibrium as reported previously [16].  $k_{\text{obs}} = (k_2 K_1[\text{PR}_3]) / (1 + K_1[\text{PR}_3])$ ;  $k_{\text{obs}}$  represents the *pseudo*-first order rate constant ( $[\text{P}] \gg [\text{Fe}]$ ).

Firstly, the electronic character of the M-PR<sub>3</sub> bond which is a combined effect of the  $\sigma$ -bond formed by donation of lone pair electrons from the phosphine ligand to the metal atom, and the ability of the phosphine ligand to accept electron density from the metal back into the appropriate phosphine orbital [10]. The  $\sigma$ -basicity and  $\pi$ -acidity of the phosphorous ligand has been studied by Tolman by comparing the carbonyl stretching absorption bands of the coordinated CO ligands in  $[\text{Ni}(\text{CO})_3(\text{PR}_3)]$  complexes [11]. Strong  $\sigma$ -donor ligands give a high electron density on the metal centre and therefore a substantial back-donation to the CO ligands and lowered IR frequencies. Strong  $\pi$ -acceptor ligands on the other hand, compete with CO for the electron back-donation and the CO stretch frequencies remain high [7]. The  $\sigma$ -donor ability of the tertiary phosphine ligands is expected to correlate with the  $\text{p}K_{\text{a}}$  values of  $\text{HPR}_3^+$ . Substituents with better electron donating capabilities promote Lewis basicity of the phosphine, while  $\pi$ -acidity is promoted by electron withdrawing groups [12].

According to the Quantitative Analysis of Ligand Effects (QALE) hypothesis [13], the nature of the metal phosphorous bond has a strong influence on the electron density around the metal center. Strong  $\sigma$ -donors enhance the electron density, whereas  $\pi$ -acceptors decrease the electron density. This model leads to the conclusion that the Fe–P bond distance can be utilised to diagnose the  $\sigma$ -donor or a  $\pi$ -acceptor character of the phosphine ligand. It predicts that pure  $\sigma$ -donor ligands exhibit long Fe–P bond distances of ca. 2.20 Å whereas  $\sigma$  donor/ $\pi$ -acceptor ligands should have shorter distances of ca. 2.10 Å [14]. The here reported acyl complexes  $[\text{CpFe}(\text{CO})(\text{COMe})\text{PR}_3]$  (R = 4-FC<sub>6</sub>H<sub>4</sub> in **2a** and 4-MeC<sub>6</sub>H<sub>4</sub> in **2b**) are crystalline materials and consequently, characterised by X-ray crystallography to evaluate both the electronic and steric properties of the ligands.

Previous kinetic studies indicated a mechanism in which alkyl migration in  $[\text{CpFe}(\text{CO})_2\text{Me}]$  from metal to CO occurs in the first step and an unsaturated 16-electron, or solvent saturated acyl intermediate, complex is generated [15]. Attack of a nucleophile on the intermediate produces the final product. These studies showed that nucleophilic and polar solvents increase the insertion rate, and the authors attributed this effect to the stabilisation of the unsaturated intermediate by the solvent.

Bassetti and co-workers [16] proposed a mechanism in which a rapid formation of an outer-sphere complex between the alkyl complex,  $[\eta^5\text{-C}_9\text{H}_7\text{Fe}(\text{CO})_2\text{Me}]$ , and

the phosphine ligand is followed by simultaneous coordination of the phosphine ligand and migration of the alkyl group. Our long term interest into elucidation of the electronic and steric effects of Group 15 ligands [17] led us to the present study, which was conducted to structurally and kinetically investigate the electronic effects of two isosteric ligands, P(4-FC<sub>6</sub>H<sub>4</sub>)<sub>3</sub> and P(4-MeC<sub>6</sub>H<sub>4</sub>)<sub>3</sub>. The kinetics of the migratory CO insertion reaction in  $[\text{CpFe}(\text{CO})_2\text{Me}]$  (**1**), was studied using UV–vis, IR, <sup>19</sup>F and <sup>31</sup>P NMR spectroscopies, which confirmed the general two-step reaction represented in Scheme 1. The resulting products were fully characterised and their molecular structures were determined by single crystal X-ray spectroscopy.

## 2. Experimental

### 2.1. General

All syntheses of air and moisture sensitive compounds were performed using standard Schlenk techniques under prepurified N<sub>2</sub> [18]. All solvents were pre-dried by passage over alumina (neutral, Brockmann grade I). MeCN was distilled from P<sub>2</sub>O<sub>5</sub>, tetrahydrofuran from Na/benzophenone and CH<sub>2</sub>Cl<sub>2</sub> from CaH<sub>2</sub> prior to use [19].  $[\text{CpFe}(\text{CO})_2]_2$  and  $[\text{CpFe}(\text{CO})_2\text{Me}]$  (**1**), were prepared according to literature procedures [20]. Fe(CO)<sub>5</sub>, dicyclopentadiene and the phosphine ligands were obtained from Sigma–Aldrich and used as received. Melting points of **2a** and **2b** were determined on a Kofler hot-stage microscope (Reichert-Thermovar). Infrared spectra were recorded on a Bruker Equinox 55 FT-IR spectrometer and analysed with the Bruker OPUS-NT software (32 scans, 4 cm<sup>-1</sup> resolution, Blackman-Harris 3-Term apodisation). Infrared data for solution spectra of compounds **2a** and **2b** were collected using NaCl windows (optical path 0.1 mm). NMR spectra were recorded on a Varian Gemini 2000 spectrometer (<sup>1</sup>H: 300 MHz, <sup>19</sup>F: 282.3 MHz, <sup>31</sup>P: 121.5 MHz, <sup>13</sup>C: 75.5 MHz). NMR spectra were referenced relative to TMS (<sup>1</sup>H, <sup>13</sup>C), SOCF<sub>3</sub> (<sup>19</sup>F) or 85% H<sub>3</sub>PO<sub>4</sub> (<sup>31</sup>P) using either the residual protonated impurities in the solvent (<sup>1</sup>H NMR), the solvent resonance (<sup>13</sup>C NMR), or an external reference (<sup>19</sup>F, <sup>31</sup>P). UV–vis spectra were recorded on a Varian Cary 50 spectrometer equipped with a thermostated water bath accurate to 0.1° in a double-sided 1 cm tandem quartz cells with Teflon caps.

## 2.2. Structure determination

Crystals of  $[\text{CpFe}(\text{CO})(\text{COMe})\text{P}(4\text{-FC}_6\text{H}_4)_3]$  (**2a**), and  $[\text{CpFe}(\text{CO})(\text{COMe})\text{P}(4\text{-FC}_6\text{H}_4)_3]$  (**2b**), were grown from pentane as described below. X-ray diffraction data for **2a** and **2b** were collected on the Bruker SMART 1K CCD area detector diffractometer using a graphite monochromated Mo  $\text{K}\alpha$  ( $\lambda = 0.71073 \text{ \AA}$ ) collecting  $\omega$ -scans at 293(2) K. After completion, the first 50 frames were recollected to check for decay, which was not observed. All the reflections were merged and integrated using SAINT+ [21]. The structures were solved by the heavy atom method and refined through full-matrix least squares cycles using the SHELXL-97 [22] software package with  $\sum(|F_o| - |F_c|)^2$  being minimised. All non-H atoms were refined with anisotropic displacement parameters, while the H atoms were constrained to parent sites using a riding model. The Diamond Visual Crystal Structure information system software was used for the graphics [23]. Crystal data and details of data collection and refinement are presented in Table 1. CCDC reference numbers 269347 and 269348. See <http://www.ccdc.cam.ac.uk>.

2.3. Preparation of  $[\text{CpFe}(\text{CO})(\text{COMe})\text{P}(4\text{-FC}_6\text{H}_4)_3]$  (**2a**)

A solution of  $\text{P}(4\text{-FC}_6\text{H}_4)_3$  (160 mg, 0.5 mmol) in MeCN (2.0 ml) was added to a solution of **1** (100 mg, 0.5 mmol) in MeCN (2.0 ml). The mixture was heated under reflux for ca. 48 h. The solvent was evaporated in vacuo and the residue dissolved in acetone and pentane (1:20). The product was purified by column chromatography over silica, eluting with hexane. The first yellow band ( $R_f = 0.34$ ) was collected. Evaporation of the solvent gave crude **2a** as a crystalline yellow material. Recrystallisation from pentane afforded crystals suitable for X-ray studies. (0.14 g, 50%) m.p. 151 °C.  $\nu_{\text{max}}/\text{cm}^{-1}$  ( $\text{CHCl}_3$ ) 1918 (CO);  $\nu_{\text{max}}/\text{cm}^{-1}$  (KBr) 1904 (CO) 1607 (COMe);  $\delta_{\{\text{H}\}}$  ( $\text{CDCl}_3$ , 300 MHz,) 2.32 (3H, s,  $\text{COCH}_3$ ), 4.39 (5H, s,  $\text{C}_5\text{H}_5$ ), 7.05–7.68 (12H, m,  $\text{C}_6\text{H}_4$ );  $\delta_{F\{\text{H}\}}$  ( $\text{CDCl}_3$ , 282.3 MHz)  $-112.30$ ;  $\delta_{P\{\text{H}\}}$  ( $\text{CDCl}_3$ , 121.5 MHz) 75.40;  $\delta_{C\{\text{H}\}}$  ( $\text{CDCl}_3$ , 75.5 MHz) 52.5 ( $\text{COCH}_3$ ), 85.6 ( $\text{C}_5\text{H}_5$ ), 115.9 (dd,  $J = 10 \text{ Hz}$ , 3,5- $\text{C}_6\text{H}_4$ ), 128.4 (d,  $J = 9 \text{ Hz}$ ,  $\text{C}_6\text{H}_4$ ), 133.6 (t,  $J = 10 \text{ Hz}$ , 4- $\text{C}_6\text{H}_4$ ), 135.7 (t,  $J = 10 \text{ Hz}$ , 2,6- $\text{C}_6\text{H}_4$ ), CO and COMe were not observed;  $\lambda_{\text{max}}/\text{nm}$  ( $\text{CH}_2\text{Cl}_2$ )

Table 1

Crystal data and structural refinement for  $[\text{CpFe}(\text{CO})(\text{COMe})\text{P}(4\text{-FC}_6\text{H}_4)_3]$  (**2a**) and  $[\text{CpFe}(\text{CO})(\text{COMe})\text{P}(4\text{-MeC}_6\text{H}_4)_3]$  (**2b**)

	<b>2a</b>	<b>2b</b>
Empirical formula	$\text{C}_{26}\text{H}_{20}\text{F}_3\text{FeO}_2\text{P}$	$\text{C}_{26}\text{H}_{29}\text{FeO}_2\text{P}$
Formula weight	508.24	496.34
$T$ (K)	293(2)	293(2)
Wavelength $\text{\AA}$	0.71073	0.71073
Crystal system	Triclinic	Triclinic
Space group	$P\bar{1}$	$P\bar{1}$
$a$ ( $\text{\AA}$ )	8.2497(16)	8.256(3)
$b$ ( $\text{\AA}$ )	8.7164(17)	9.552(3)
$c$ ( $\text{\AA}$ )	16.655(3)	17.245(6)
$\alpha$ ( $^\circ$ )	80.074(4)	106.063(6)
$\beta$ ( $^\circ$ )	78.618(4)	91.285(9)
$\gamma$ ( $^\circ$ )	86.783(3)	98.721(6)
$V$ ( $\text{\AA}^3$ )	1156.2(4)	1288.9(7)
$Z$	2	2
Calculated density ( $\text{mg m}^{-3}$ )	1.460	1.279
Absorption coefficient ( $\text{mm}^{-1}$ )	0.766	0.670
$F(000)$	520	520
Crystal size (mm)	$0.38 \times 0.20 \times 0.18$	$0.46 \times 0.22 \times 0.16$
$\theta$ Range ( $^\circ$ )	1.26–26.50	1.23–26.00
Index ranges	$-10 \leq h \leq 10$ $-10 \leq k \leq 10$ $-20 \leq l \leq 14$	$-9 \leq h \leq 10$ $-11 \leq k \leq 10$ $-21 \leq l \leq 20$
Collected reflections	7236	7735
Unique reflections	4759	5019
Observed reflections	3646	3758
$R_{\text{int}}$	0.0404	0.0224
Completeness to $2\theta$	99.2%	99.00%
Refinement method	Full-matrix least-squares on $F^2$	Full-matrix least-squares on $F^2$
Data/restraints/parameters	4759/0/299	5019/0/302
Goodness-of-fit on $F^2$	1.031	1.078
Final $R_1$ indices [ $I > 2\sigma(I)$ ]	$R_1 = 0.0392$ , $wR_2 = 0.0997$	$R_1 = 0.0357$ , $wR_2 = 0.0881$
$R_1$ (all data)	$R_1 = 0.0566$ , $wR_2 = 0.1080$	$R_1 = 0.0537$ , $wR_2 = 0.1056$
Largest different peak and hole ( $\text{e \AA}^{-3}$ )	0.411 and $-0.256$	0.291 and $-0.214$

337.7 ( $\epsilon$  1168  $\text{M}^{-1} \text{cm}^{-1}$ );  $\lambda_{\text{max}}/\text{nm}$  ( $\text{CH}_3\text{CN}$ ) 336.55 ( $\epsilon$  2417  $\text{M}^{-1} \text{cm}^{-1}$ ).

#### 2.4. Preparation of $[\text{CpFe}(\text{CO})(\text{COMe})\text{P}(4\text{-FC}_6\text{H}_4)_3]$ (**2b**)

A solution of  $\text{P}(4\text{-MeC}_6\text{H}_4)_3$  (150 mg, 0.5 mmol) in MeCN (2.0 ml) was added to a solution of **1** (100 mg, 0.5 mmol) in MeCN (2.0 ml). The mixture was heated under reflux for ca. 72 h after which the reaction mixture was cooled and filtered. The product was purified by column chromatography over silica eluting with hexane:acetone = 9:1. The yellow band ( $R_f = 0.28$ ) was collected. Evaporation of the solvent gave the title compound as an orange crystalline material. Recrystallisation from pentane afforded crystals suitable for X-ray studies. (0.23 g, 80%) m.p. 156 °C.  $\nu_{\text{max}}/\text{cm}^{-1}$  ( $\text{CHCl}_3$ ) 1915 (CO);  $\nu_{\text{max}}/\text{cm}^{-1}$  (KBr) 1898 (CO), 1597 ( $\text{COCH}_3$ );  $\delta_{\{\text{H}\}}$  ( $\text{CDCl}_3$ , 300 MHz) 2.30 (3H, s,  $\text{COCH}_3$ ) 2.33 (9H, s,  $\text{CH}_3\text{C}_6\text{H}_4$ ), 4.38 (5H, s,  $\text{C}_5\text{H}_5$ ), 7.30–7.38 (12H, m,  $\text{C}_6\text{H}_4$ );  $\delta_{\text{P}\{\text{H}\}}$  ( $\text{CDCl}_3$ , 121.5 MHz) 73.68;  $\delta_{\text{C}\{\text{H}\}}$  ( $\text{CDCl}_3$ , 75.5 MHz) 21.7 ( $\text{C}_3$ ), 52.3 ( $\text{COCH}_3$ ), 88.6 ( $\text{C}_5\text{H}_5$ ), 128.5 ( $^4J = 9$  Hz, 4- $\text{C}_6\text{H}_4$ ), 129.2 ( $^3J = 10$  Hz, 3,5- $\text{C}_6\text{H}_4$ ), 133.6 ( $^2J = 10$  Hz, 2,6- $\text{C}_6\text{H}_4$ ), 136.9 ( $^1J = 43$  Hz, 1- $\text{C}_6\text{H}_4$ ), CO and COMe were not observed;  $\lambda_{\text{max}}/\text{nm}$  ( $\text{CH}_2\text{Cl}_2$ ) 334.7 ( $\epsilon$  2514  $\text{M}^{-1} \text{cm}^{-1}$ );  $\lambda_{\text{max}}/\text{nm}$  ( $\text{CH}_3\text{CN}$ ) 326.4 ( $\epsilon$  4588  $\text{M}^{-1} \text{cm}^{-1}$ ).

#### 2.5. Kinetics studies

##### 2.5.1. NMR and IR spectroscopies

A mixture of alkyl complex **1** (31 mM) and  $\text{P}(4\text{-FC}_6\text{H}_4)_3$  or  $\text{P}(4\text{-MeC}_6\text{H}_4)_3$  (120/140 mM) in MeCN was thermostated at 58.0 °C. Aliquots (0.10 ml) were taken at timed intervals of ca. 3 h for  $\text{P}(4\text{-MeC}_6\text{H}_4)_3$ , or ca. 10 h for  $\text{P}(4\text{-FC}_6\text{H}_4)_3$ , and thermally quenched by storage under inert atmosphere below 10 °C. All samples were analysed at the end of the kinetic run and reconstituted with  $\text{CDCl}_3$ .

##### 2.5.2. UV-vis studies

Kinetic measurements were carried out by UV-vis spectroscopy on a Varian Cary-50 spectrometer at 50.0 °C under pseudo-first order conditions, using an excess of phosphine ligand. Blank experiments on solutions of alkyl complex **1** in the absence of ligand showed no significant decomposition during the time required for the kinetic runs.

Complex **1** (0.52 mM) and a set of  $\text{P}(4\text{-FC}_6\text{H}_4)_3$  or  $\text{P}(4\text{-MeC}_6\text{H}_4)_3$  solutions, ranging in  $[\text{P}(4\text{-FC}_6\text{H}_4)_3]$  from 5.0150 mM (or  $[\text{P}(4\text{-FC}_6\text{H}_4)_3]$  from 3.3–26.3 mM), in MeCN were added to different compartments of tandem quartz cells. The cells were stoppered and placed into a thermostated cell holder. Time was allowed for thermal equilibration before the cells were shaken to ensure mixing of the two solutions. The resulting mixture was

immediately placed in the spectrometer and the spectral change was recorded in the wavelength range of 200–600 nm. Least-squares data analyses for the individual runs, using first order kinetics and the limiting rate law as reported in the literature [16] were conducted by means of MicroMath Scientist [24].

### 3. Results and discussion

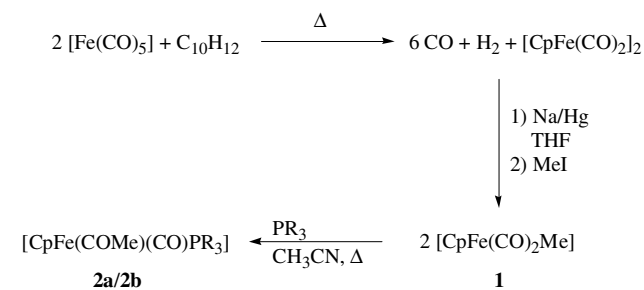
#### 3.1. Synthesis

Scheme 2 outlines the overall procedure for the synthesis of complexes **1**, **2a** and **2b**. Complex **1** was prepared by reduction of the iron carbonyl dimer  $[\text{CpFe}(\text{CO})_2]_2$  with excess sodium amalgam, followed by reaction with methyl iodide [20]. The product was isolated as a moderately oxygen sensitive yellow crystalline material.

Treatment of one equivalent of the alkyl complex **1** with one equivalent of the phosphine ligand  $\text{P}(4\text{-FC}_6\text{H}_4)_3$  or  $\text{P}(4\text{-MeC}_6\text{H}_4)_3$  in acetonitrile gives the corresponding acyl complexes  $[\text{CpFe}(\text{CO})(\text{COMe})\text{P}(4\text{-FC}_6\text{H}_4)_3]$  (**2a**) and  $[\text{CpFe}(\text{CO})(\text{COMe})\text{P}(4\text{-MeC}_6\text{H}_4)_3]$  (**2b**), in moderate to good yields. The products were isolated as air stable, orange crystalline materials which slowly decompose in solution.

IR spectroscopy of the two complexes showed the expected  $\nu_{\text{CO}}$  absorption bands at 1904 and 1898  $\text{cm}^{-1}$  for **2a** and **2b**, respectively. The acyl  $\nu_{\text{CO}}$  absorptions bands are observed at 1607 and 1597  $\text{cm}^{-1}$  for **2a** and **2b**, respectively. The complexes **2a** [13,25] and **2b** [13,25,26] were reported previously, but only  $\nu_{\text{CO}}$  absorption bands in cyclohexane were reported ( $\nu_{\text{CO}} = 1924$  for **2a** and 1920 for **2b**).

Upon methyl migration, one of the CO groups is replaced by a phosphine ligand inducing the formation of the acetyl group. Consequently the electron density on the metal center increases, leading to the lowering of the  $\nu_{\text{CO}}$  absorption band due to increased Fe–CO bond order. In **2a** compared to **2b** the  $\nu_{\text{CO}}$  absorption band is shifted to a lower value which is a good indication that  $\text{P}(4\text{-MeC}_6\text{H}_4)_3$  in complex **2b** is a better  $\sigma$ -donor than



Scheme 2. The sequence for the synthesis of **2a** and **2b**.  $\text{PR}_3 = \text{P}(4\text{-FC}_6\text{H}_4)_3$  (**2a**),  $\text{P}(4\text{-MeC}_6\text{H}_4)_3$  (**2b**).

P(4-FC<sub>6</sub>H<sub>4</sub>) in **2a**. An upfield shift of the Cp protons in the <sup>1</sup>H NMR, from  $\delta$  4.73 ppm in **1** to  $\delta$  4.39 ppm in **2a** and  $\delta$  4.38 ppm in **2b** was also observed.

In the <sup>31</sup>P NMR spectrum, complex **2a** is observed at  $\delta$  75.40 ppm and **2b** at 73.68 ppm, while the respective free ligands resonate at  $\delta$  8.5 ppm (P(4-FC<sub>6</sub>H<sub>4</sub>)<sub>3</sub>) and  $\delta$  7.6 ppm (P(4-MeC<sub>6</sub>H<sub>4</sub>)<sub>3</sub>). Extra peaks were observed in the <sup>31</sup>P spectrum during kinetic runs at  $\delta$  27.50 and  $\delta$  29.67 ppm and these were found to correspond to the phosphine oxides.

### 3.2. X-ray crystallography results

Orange crystals of **2a** and **2b** were characterised by X-ray crystallography and the numbering scheme of both **2a** and **2b** are presented in Figs. 1 and 2, respectively. The bond distances and angles of interest are presented in Table 2.

In both structures, the molecules pack in the triclinic  $P\bar{1}$  ( $Z = 2$ ) space group. The Cp ring is centrally bound above the plane of the metal centre and the other ligands are pointing down like the legs of a three-legged “bar stool”. The iron atom adopts a pseudo-octahedral coordination geometry; the Cp ring occupying three coordination sites with the remaining three ligands oriented perpendicular to each other. In **2a** the packing is stabilised by selective hydrogen interactions between the fluorine and appropriate hydrogen atoms of the neighbouring molecules (see Table 3).

The Fe–P bond distances of **2a** and **2b** are, surprisingly, the same at 2.1932(8) Å (see Table 2). Other similarities between **2a** and **2b**, for example the Fe–Cp bond

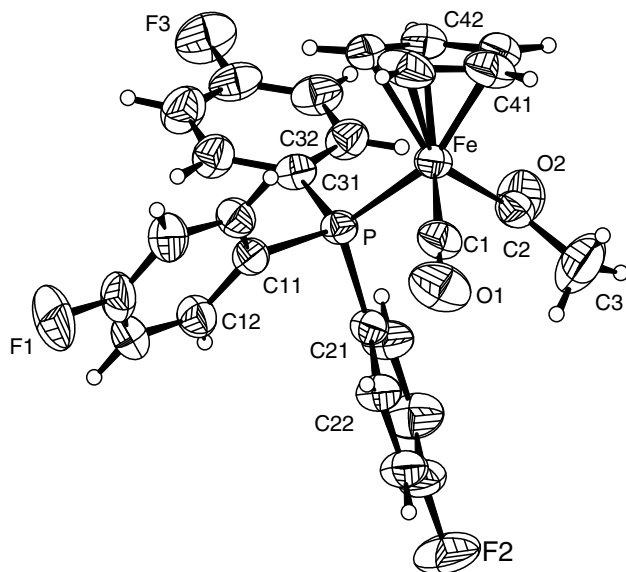


Fig. 1. X-ray crystal structure of [CpFe(CO)(COMe)P(4-FC<sub>6</sub>H<sub>4</sub>)<sub>3</sub>] (**2a**) (50% probability). For the aromatic rings, the first digit refers to the ring number while the second digit indicates the number of the C-atom in the ring.

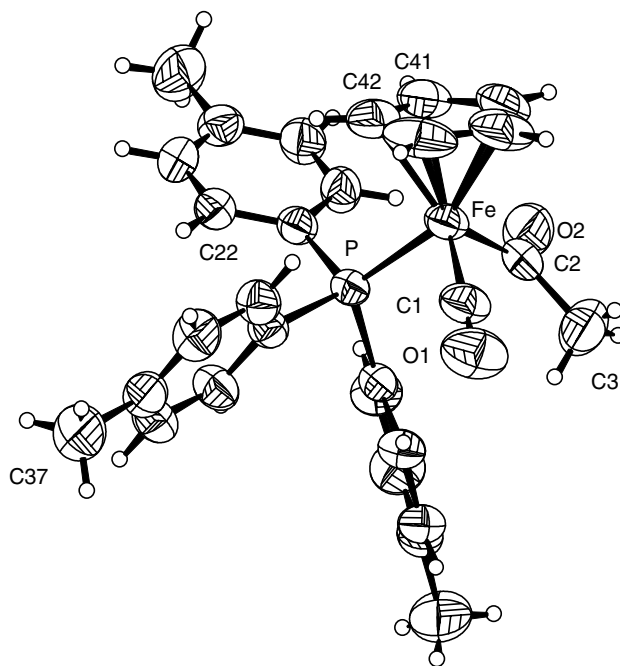


Fig. 2. X-ray crystal structure of [CpFe(CO)(COMe)P(4-MeC<sub>6</sub>H<sub>4</sub>)<sub>3</sub>] (**2b**) (50% probability). For the aromatic rings, the first digit refers to the ring number while the second digit indicates the number of the C-atom in the ring.

Table 2  
Selected interatomic bond distances (Å) and angles (°) for [CpFe(CO)(COMe)P(4-FC<sub>6</sub>H<sub>4</sub>)<sub>3</sub>] (**2a**) and [CpFe(CO)(COMe)P(4-MeC<sub>6</sub>H<sub>4</sub>)<sub>3</sub>] (**2b**)

	<b>2a</b>	<b>2b</b>
<i>Distances (Å)</i>		
Fe–C(1)	1.748(3)	1.744(3)
Fe–C(2)	1.955(3)	1.951(3)
Fe–P	2.1932(8)	2.1932(8)
C(1)–O(1)	1.150(3)	1.149(3)
C(2)–O(2)	1.201(3)	1.200(3)
C(2)–C(3)	1.521(4)	1.538(4)
Fe–centroid	1.749(4)	1.752(7)
<i>Angles (°)</i>		
C(1)–Fe–C(2)	94.41(12)	94.77(12)
C(1)–Fe–P	91.69(9)	93.07(8)
C(2)–Fe–P	90.12(9)	89.03(8)
O(1)–C(1)–Fe	174.3(3)	174.3(2)
Cp–Fe–P	127.4(2)	125.9(1)
Cp–Fe–C(1)	124.7(1)	124.1(2)
Cp–Fe–C(2)	119.1(1)	120.7(2)
<i>Torsion angle (°)</i>		
O(2)–C(2)–Fe–C1	156.5(3)	170.3(5)
C(1)–Fe–P–C(11)	54.6(1)	–62.5(1)
C(1)–Fe–P–C(21)	–62.4(1)	174.5(1)
C(1)–Fe–P–C(31)	175.2(1)	54.0(1)
C(2)–Fe–P–C(11)	149.1(1)	32.2(1)
C(2)–Fe–P–C(21)	32.0(1)	–90.7(1)
C(2)–Fe–P–C(31)	–90.4(1)	148.7(1)
<i>Dihedral angles (°)</i>		
Plane 1 and 2 <sup>a</sup>	8.1(2)	7.0(4)

<sup>a</sup> Plane 1 is the plane of the Cp ring and plane 2 is described by P, C(1) and C(2).

Table 3

Inter- and intramolecular hydrogen bond distances (Å) and angles (°) for [CpFe(CO)(COMe)P(4-FC<sub>6</sub>H<sub>4</sub>)<sub>3</sub>] (**2a**) and [CpFe(CO)(COMe)P(4-MeC<sub>6</sub>H<sub>4</sub>)<sub>3</sub>] (**2b**)

D–H···A	D–H	H···A	D···A	∠(DHA)
For <b>2a</b>				
C23–H23...O2 <sup>a</sup>	0.93	2.57	3.420(4)	153.0
C32–H32...O2	0.93	2.39	3.252(4)	154.0
C33–H33...F2 <sup>b</sup>	0.93	2.54	3.383(3)	150.9
C42–H42...F1 <sup>c</sup>	0.93	2.52	3.379(3)	153.3
For <b>2b</b>				
C13–H13...O2 <sup>a</sup>	0.93	2.49	3.370(4)	157.0
C26–H26...O2	0.93	2.45	3.302(4)	153.1

<sup>a</sup> 1 + x, y, z.

<sup>b</sup> 1 – x, 1 – y, –z.

<sup>c</sup> –1 + x, 1 + y, z.

distances (1.748(3) for **2a** and 1.744(3) for **2b**), are listed in Table 2.

The most widely used method for determining ligand steric behaviour at a metal centre is the calculation of the Tolman cone angle [11], using an M–P bond distance of 2.28 Å, C–H bond distances of 0.97 Å and a Van der Waals radius of 1.2 Å for the H atoms. For this study actual Fe–P bond distances were used, yielding effective cone angles  $\theta_E$  of 152° for P(4-FC<sub>6</sub>H<sub>4</sub>)<sub>3</sub> and 153° for P(4-MeC<sub>6</sub>H<sub>4</sub>)<sub>3</sub> [27]. The effective cone angles are slightly larger than the Tolman cone angles (145° for both ligands [11]) due to the shorter M–P bond distance.

Since the effective angles  $\theta_E$  of P(4-FC<sub>6</sub>H<sub>4</sub>)<sub>3</sub> and P(4-MeC<sub>6</sub>H<sub>4</sub>)<sub>3</sub> are comparable, it is to be expected that their respective steric environments are similar. This is exemplified in the Cp(centroid)–Fe–P angle, which remains the same for both phosphine ligands.

In the QALE [14] hypothesis, P(C<sub>6</sub>H<sub>5</sub>)<sub>3</sub> is classified as a pure  $\sigma$ -donor because it exhibits a comparatively long Fe–P bond distance (see Table 4). The two ligands in **2a** and **2b** can thus also be classified as pure  $\sigma$ -donors, because their bond distances are similar to that of P(C<sub>6</sub>H<sub>5</sub>)<sub>3</sub>. The Fe(CO) and Fe(COMe) bond distances for complexes **2a** and **2b** are longer compared to that

of the triphenylphosphine analogues (Table 4 [14]), while the rest of the bond distances are similar. However, smaller  $\pi$ -acceptor properties of these ligands, although not easily detected, should never be ignored completely.

The acyl oxygen is orientated anti to the carbonyl oxygen in both complexes with torsion angles of 156.5(3)° and 170.3(5)° for **2a** and **2b**, respectively. This was probably due to the steric interaction between the acyl ligand and the phenyl rings on the phosphine. A similar observation was reported by Davies et al. [28] for the P(C<sub>6</sub>H<sub>5</sub>)<sub>3</sub> analogue.

### 3.3. Kinetic results

The complex [CpFe(CO)<sub>2</sub>Me] (**1**) reacted with P(4-FC<sub>6</sub>H<sub>4</sub>)<sub>3</sub> and P(4-MeC<sub>6</sub>H<sub>4</sub>)<sub>3</sub> in acetonitrile to give the corresponding acyl complexes [CpFe(CO)(COMe)P(4-FC<sub>6</sub>H<sub>4</sub>)<sub>3</sub>] (**2a**) and [CpFe(CO)(COMe)P(4-MeC<sub>6</sub>H<sub>4</sub>)<sub>3</sub>] (**2b**), as the unique metal complexes. Both the starting materials and the products were fully characterised and the reactions were spectroscopically quantitative (IR, NMR).

The kinetic runs were carried out under pseudo-first-order conditions using a large excess of phosphine. The reactions were followed at 50.0 °C by monitoring the increase in absorbance at ca. 360 nm in the UV–vis due to product formation. In addition to the UV–vis kinetics, the reactions were followed by IR spectroscopy at 58.0 °C. The decrease in absorbance at 2006 and 1946 cm<sup>-1</sup>  $\nu_{CO}$  for **1**), as well as the increase in absorbance of the  $\nu_{CO}$  for **2a** and **2b**, at 1918 and 1915 cm<sup>-1</sup>, respectively, were monitored. The rates were obtained as an average for the rate of the disappearance of the two  $\nu_{CO}$  absorption bands for **1**, and the rate of formation of the  $\nu_{CO}$  absorption bands of the products.

The reaction for **2a** was additionally followed using <sup>19</sup>F NMR spectroscopy at 58 °C and the spectral change is presented in Fig. 3. The changes in the <sup>19</sup>F NMR spectra are characterised by the disappearance of the signal

Table 4

Structural correlations for the complexes of the type [CpFe(CO)(COMe)PR<sub>3</sub>] [14]

	<b>2a</b>	<b>2b</b>	[CpFe(CO)(COMe)P(C <sub>6</sub> H <sub>5</sub> ) <sub>3</sub> ]	[Cp'Fe(CO)(COMe)P(C <sub>6</sub> H <sub>5</sub> ) <sub>3</sub> ]
Fe–P	2.1932(8)	2.1932(8)	2.202(2)	2.195(3)
Fe–C(O)	1.748(3)	1.744(3)	1.708(2)	1.694(10)
Fe–C(=O)	1.955(3)	1.951(3)	1.917(8)	1.921(9)
Fe–Cp <sup>a</sup>	1.748(4)	1.751(7)	1.752(5)	1.746(8)
Fe–Cp <sup>b</sup>	2.118(6)	2.113(6)	2.118(11)	2.114(10)
$\theta_E$	152	153	159	159
Reference	<sup>d</sup>	<sup>d</sup>	<sup>e</sup>	<sup>e</sup>

Cp' = MeC<sub>5</sub>H<sub>4</sub>.

<sup>a</sup> The centroid of the Cp ring.

<sup>b</sup> The average Fe–C(Cp) distances.

<sup>d</sup> This work.

<sup>e</sup> Reference [14].

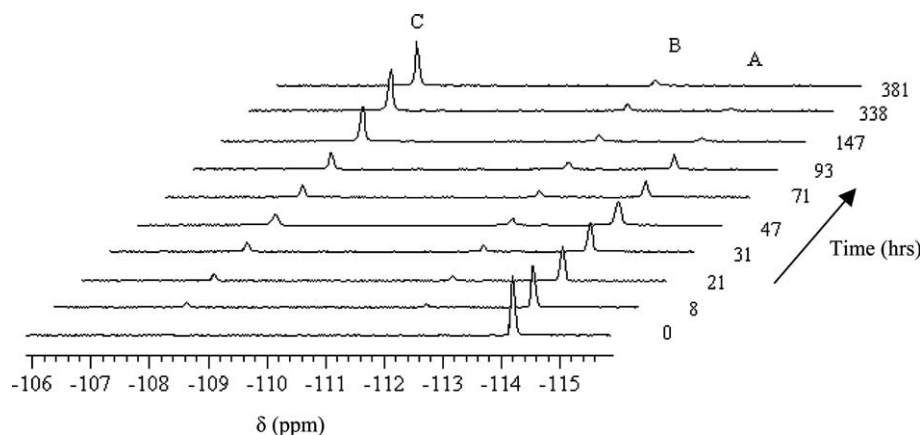


Fig. 3. The  $^{19}\text{F}$  NMR spectral change during the reaction of  $[\text{CpFe}(\text{CO})_2\text{Me}]$  (**1**), (31 mM) with  $\text{P}(4\text{-FC}_6\text{H}_4)_3$ , A, (120 mM) yielding  $[\text{CpFe}(\text{CO})(\text{COMe})\text{P}(4\text{-FC}_6\text{H}_4)_3]$  (**2a**) (B) in MeCN at  $58.0^\circ\text{C}$ .

for the non-coordinated phosphine (A) at  $\delta$  114 ppm and the formation of the acetyl complex **2a** at  $\delta$  112 ppm. The formation of the acetyl complex is accompanied by the formation of phosphine oxide, observed at  $\delta$  108 ppm (C). A kinetic plot of the integration of the various peaks in the  $^{19}\text{F}$  NMR vs. time is presented in Fig. 4. In agreement with these results, the  $^{31}\text{P}$  NMR spectral change showed the formation of the acetyl complex **2a** at  $\delta$  75.4 ppm with the uncoordinated phosphine ligand resonating at  $\delta$  8.5 ppm, while the corresponding phosphine oxide was observed at  $\delta$  27.5 ppm.

The reactions were first-order in the methyl complex  $[\text{CpFe}(\text{CO})_2\text{Me}]$  (**1**), while the dependence of the rate on phosphine concentration follows a non-linear behaviour. With increasing concentration of the phosphine, the reactivity tends toward a limiting rate (saturation kinetics) in agreement with Scheme 1. The rate constants

obtained in acetonitrile were  $k_2 = (3.4 \pm 0.4) \times 10^{-5} \text{ s}^{-1}$  for  $\text{P}(4\text{-MeC}_6\text{H}_4)_3$  and  $k_2 = (2.2 \pm 0.2) \times 10^{-6} \text{ s}^{-1}$  for  $\text{P}(4\text{-FC}_6\text{H}_4)_3$ . The same non-linear dependence on phosphine concentration was reported by Bassetti and coworkers for the migratory carbonyl insertion of  $[\eta^5\text{-C}_9\text{H}_7\text{Fe}(\text{CO})_2\text{Me}]$  [16].

The general trend we found, that the  $\text{P}(4\text{-MeC}_6\text{H}_4)_3$  ligand is faster than the  $\text{P}(4\text{-FC}_6\text{H}_4)_3$  ligand is in broad agreement with literature, though it is difficult to directly compare our study with the literature results.

Upon changing the solvent from acetonitrile to dichloromethane for  $\text{P}(4\text{-MeC}_6\text{H}_4)_3$ , similar saturation kinetics was observed at  $30.0^\circ\text{C}$ , with a rate of  $k_2 = (2.2 \pm 0.5) \times 10^{-6} \text{ s}^{-1}$ . If 'normal' activation energy holds, a constant for acetonitrile at  $30^\circ\text{C}$  of ca.  $7 \times 10^{-6} \text{ s}^{-1}$  is calculated for the  $\text{P}(4\text{-MeC}_6\text{H}_4)_3$  complex. This is ca. three times more rapid than in dichloromethane.

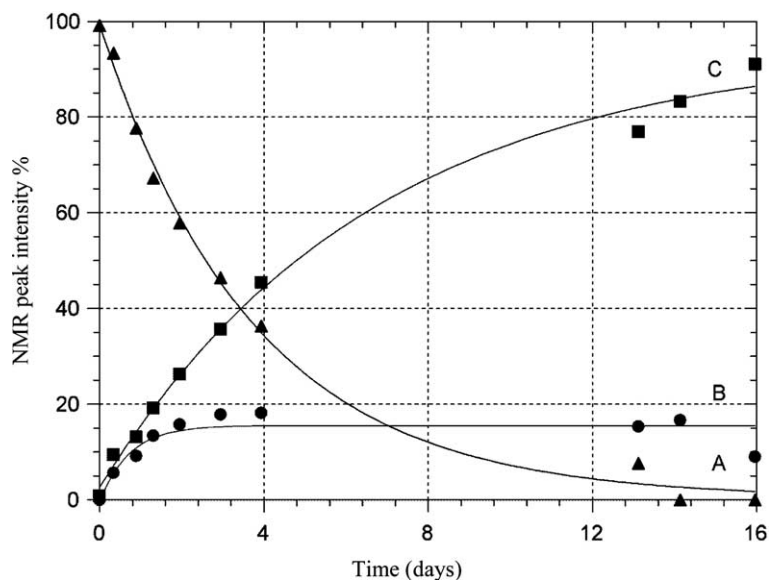


Fig. 4. Increase and decrease of the  $^{19}\text{F}$  NMR peak intensities for the reaction of  $[\text{CpFe}(\text{CO})_2\text{Me}]$  (**1**) (31 mM) with  $[\text{P}(4\text{-FC}_6\text{H}_4)_3]$  (120 mM) yielding  $[\text{CpFe}(\text{CO})(\text{COMe})\text{P}(4\text{-FC}_6\text{H}_4)_3]$  (**2a**) in MeCN at  $58^\circ\text{C}$  ( $\blacktriangle$  =  $\text{P}(4\text{-FC}_6\text{H}_4)_3$ ,  $\bullet$  =  $[\text{CpFe}(\text{CO})(\text{COMe})\text{P}(4\text{-FC}_6\text{H}_4)_3]$ ,  $\blacksquare$  =  $\text{OP}(4\text{-FC}_6\text{H}_4)_3$ ).

Thus we conclude that increased solvent donor ability/polarity enhances the reaction rate. We can therefore also not exclude nucleophilic assistance by the solvent, or the formation of solvent-coordinated intermediates for the overall process.

Bassetti and coworkers [16] studied the migratory carbonyl insertion of  $[\eta^5\text{-C}_9\text{H}_7\text{Fe}(\text{CO})_2\text{Me}]$  using a series of *para*-substituted phosphines  $\text{P}(4\text{-XC}_6\text{H}_4)_3$  (X = H, Cl, F, OMe). However, they found no significant change of rate with increasing donor-capacity of the ligand, the differences being within experimental errors for the system. Besides the relatively small differences, they performed their studies in toluene to minimise any solvent assisted mechanisms. In addition they used the indenyl spectator ligand, instead of cyclopentadienyl, which has the ability of  $\eta^3$ -coordination in intermediates, although they did not find any evidence of a haptotropic shift.

The reaction of  $[\text{CpFe}(\text{CO})_2\text{Me}]$  with a series of  $\text{PPh}_3$ ,  $\text{PPh}_2\text{Me}$ ,  $\text{PPhMe}_2$  was reported by Bassetti and coworkers [16c]. In this study, an increase in reaction rate was observed with ligands of increasing basicity. However, these phosphines are not *iso*-steric and it is difficult to quantify the steric influence on the migratory CO insertion reaction. The same study reports on the migratory CO insertion in  $[\text{CpFe}(\text{CO})_2^i\text{Pr}]$  complexes, but the possibility of a different mechanism cannot be excluded. In general, the reaction rates of the migratory CO insertion increase when going from Me to <sup>i</sup>Pr. The <sup>i</sup>Pr group is, however, sterically significantly larger than the Me group, and it also opens up mechanistic pathways involving agostic interactions with the  $\beta$ -hydrogens. It is known from literature that a significant increase in rate is seen on substituting Me groups for higher n-alkanes, with the highest rate for an Et group [6].

One observation made during our studies is that all excess phosphine ligand is oxidised as the reaction proceeds. Part of the products, **2a** and **2b**, also decomposes in solution (see Fig. 4B). This decomposition product was not analysed further. In an earlier study conducted by Su and Wojcicki [29], it was shown that the thermal reaction between  $[\text{CpFe}(\text{CO})_2\text{R}]$  (where R = Me or Et) and  $\text{P}(\text{C}_6\text{H}_5)_3$  in hexane (69 °C) and heptane (98 °C) produced the acetyl complex  $[\text{CpFe}(\text{CO})(\text{COR})\text{P}(\text{C}_6\text{H}_5)_3]$ . Over an extended period of time this complex undergoes decarbonylation to form  $[\text{CpFe}(\text{CO})(\text{R})\text{P}(\text{C}_6\text{H}_5)_3]$ . In our studies we did not observe the decarbonylation product,  $[\text{CpFe}(\text{CO})(\text{Me})\text{P}(4\text{-FC}_6\text{H}_4)_3]$  (see Fig. 3), however we did find significant amounts of the phosphine oxides.

In order to ascertain the origin of the phosphine oxide, a blank reaction was performed which contained only the ligand and the solvent under the same conditions as that of the reaction. NMR spectra of the ligand showed a negligible degree of oxidation. Upon exposure to air it was found that only ca. 7% of the phosphine ligand oxidised after five days of heating. In the presence of alkyl complex

**1**, and insertion product **2**, the same amount of oxidation is observed within 7 h. In five days, half of the amount of the phosphine ligand used is oxidised (see Figs. 3 and 4 peaks A and C). This lead us to believe that either complex **1** or its insertion product **2** catalyses the oxidation of phosphine ligand in the present system. The formed phosphine oxides appears to have no influence on the CO migratory insertion reaction (see Fig. 4). This observation is in agreement with literature [16a].

In conclusion, the system reported here is complicated by a number of factors. First of all, the oxidation of phosphine ligand decreases the effective ligand concentration making kinetic results difficult to interpret. In addition, proper comparison with literature reports is not easy due to the small body of work performed on the system. Where reports in literature exist, they either report on systems with different spectator ligands or phosphines that vary in both steric and electronic properties. Finally, the rates of the reactions (in some cases >10 days) make accurate kinetic measurements difficult. To utilise the current system as a convenient probe to evaluate electronic characteristics of Group 15 ligands, therefore requires significant modification of reaction conditions, which is to be explored in future.

Nevertheless, the different reactants and products in Scheme 1 were accurately identified and characterised in this study, and the preliminary kinetics determined indicates that this system can in principle be used as a kinetic probe for evaluation of electronic and steric effects of Group 15 ligands.

## Acknowledgements

Financial support from the Research Funds of the University of the Free State and the University of Johannesburg are gratefully acknowledged. Part of this material is based on work supported by the South African National Research Foundation [SA NRF, GUN 2053397 (University of Johannesburg) and 2068915 (University of the Free State)]. Any opinion, findings, and conclusions or recommendations expressed in this material are those of the authors and do not necessarily reflect the views of the SA NRF. We thank Prof. D. Levendis and Dr. D. Billing (University of the Witwatersrand) for the use of their diffractometer.

## References

- [1] L.S. Hegeudus, Transition Metal in the Synthesis of Complex Organic Molecules, University books, USA, 1994, p. 29.
- [2] B. Cornils, W.A. Herrmann, Applied Homogeneous Catalysis with Organometallic Compounds, vol. 2, Wiley-VCH, Weinheim, 1991, p. 521 (Chapter 3).
- [3] (a) M. Green, D.J. Westlake, J. Chem. Soc. A (1971) 367; (b) J.P. Bibler, A. Wojcicki, Inorg. Chem. 5 (1966) 889.

- [4] J.D. Cotton, M.M. Kroes, R.D. Markwell, E.A. Miles, J. Organomet. Chem. 388 (1990) 133.
- [5] M.J. Wax, R.G. Bergman, J. Am. Chem. Soc. 103 (1981) 7028.
- [6] R. George, J.M. Anderson, J.R. Moss, J. Organomet. Chem. 505 (1995) 131.
- [7] P.W.N.M. van Leeuwen, Homogeneous Catalysis: Understanding the Art, Kluwer Academic Publishers, Netherlands, 2004, p. 10.
- [8] (a) For an example of phosphite stabilised cobalt catalysts see: M. Haumann, R. Meijboom, J.R. Moss, A. Roodt, Dalton Trans. (2004) 1679;  
(b) R. Meijboom, M. Haumann, A. Roodt, L. Damoense, Helv. Chim. Acta 88 (2005) 676.
- [9] A. Riisager, R. Fehrmann, S. Flicker, R. van Hal, M. Haumann, P. Wasserscheid, Angew. Chem., Int. Ed. 44 (2005) 815.
- [10] R.H. Crabtree, Organometallic Chemistry of the Transition Metals, Wiley, New York, USA, 1988, p. 71.
- [11] C.A. Tolman, Chem. Rev. 77 (1977) 313.
- [12] B. Douglas, D. McDaniel, J. Alexander, Concepts and Models of Inorganic Chemistry, third ed., Wiley, New York, USA, 1994, p. 570.
- [13] M.M. Rahman, H.Y. Liu, K. Eriks, A. Prock, W.P. Giering, Organometallics 8 (1989) 1.
- [14] H.Y. Liu, L.L. Koh, K. Eriks, W.P. Giering, A. Prock, Acta Cryst. C 46 (1990) 51.
- [15] I.S. Buttler, F. Basolo, R.G. Pearson, Inorg. Chem. 6 (1967) 2074.
- [16] (a) M. Bassetti, L. Mannina, D. Monti, Organometallics 13 (1994) 3293;  
(b) M. Bassetti, D. Monti, J. Am. Chem. Soc. 115 (1993) 4658;  
(c) M. Allevi, M. Bassetti, C. Lo Sterzo, D. Monti, J. Chem. Soc., Dalton Trans. (1996) 3527.
- [17] (a) See for example: S. Otto, A. Roodt, Inorg. Chim. Acta 357 (2004) 1;  
(b) A. Roodt, S. Otto, G. Steyl, Coord. Chem. Rev. 245 (2003) 125.
- [18] D.F. Shriver, M.A. Drezdson, The Manipulation of Air-Sensitive Compounds, Wiley-Interscience, New York, 1986.
- [19] D.D. Perrin, W.L.F. Armarego, Purification of Laboratory Chemicals, third ed., Butterworth-Heinemann Ltd, Oxford, 1988.
- [20] R.J. Angelici, Synthesis and Techniques in Inorganic Chemistry, second ed., University Science Books, Mill Valley, CA, 1986, p. 147.
- [21] Bruker SAINT+. Version 6.02 (including XRPEP). Bruker AXS Inc., Madison, Wisconsin, USA, 1999.
- [22] G.M. Sheldrick, SHELXL97, University of Göttingen, Germany, 1997.
- [23] K. Brandenburg, M. Berndt, Diamond version 2.1e., Crystal Impact GbR, Bonn, Germany, 2001.
- [24] SCIENTIST for Windows, ver. 4.10.1998, MicroMath, Utah, USA, 1990.
- [25] (a) A.L. Fernandez, C. Reyes, A. Prock, W.P. Giering, Perkin 2 (2000) 1033;  
(b) A.L. Fernandez, T.Y. Lee, C. Reyes, A. Prock, W.P. Giering, Organometallics 17 (1998) 3169;  
(c) A. Fernandez, C. Reyes, A. Prock, W.P. Giering, Organometallics 17 (1998) 2503;  
(d) D.C. Woska, M. Wilson, J. Bartholomew, K. Eriks, A. Prock, W.P. Giering, Organometallics 11 (1992) 3343.
- [26] (a) R.T. Aplin, J. Booth, R.G. Compton, S.G. Davies, S. Jones, J.P. McNally, M.R. Metzler, W.C. Watkins, J. Chem. Soc., Perkin Trans. 2 (1999) 913;  
(b) S.G. Davies, S. Jones, M.R. Metzler, K. Yanada, R. Yanada, J. Chem. Soc., Perkin Trans. 2 (1998) 1147;  
(c) S.C. Case-Green, J.F. Costello, S.G. Davies, N. Heaton, C.J.R. Hedgecock, V.M. Humphreys, M.R. Metzler, J.C. Prime, J. Chem. Soc., Perkin Trans. 1 (1994) 933;  
(d) S.G. Davies, M.R. Metzler, W.C. Watkins, R.G. Compton, J. Booth, J.C. Elkund, J. Chem. Soc., Perkin Trans. 2 (1993) 1603.
- [27] S. Otto, A. Roodt, J. Smith, Inorg. Chim. Acta 303 (2000) 295.
- [28] S.G. Davies, J.I. Seeman, I.H. Williams, Tetrahedron Lett. 27 (1986) 619.
- [29] S.R. Su, A. Wojcicki, J. Organomet. Chem. 27 (1971) 231.